

Implications of laser-doping parameters and contact opening size on contact resistivity

Jonas D. Huyeng^{1,2}, Marco Ernst², Kean Chern Fong², Daniel Walter² and Andrew Blakers²

¹Fraunhofer Institute for Solar Energy Systems (ISE), Heidenhofstrasse 2, 79110 Freiburg, Germany

²Centre for Sustainable Energy Systems, Australian National University, Canberra, ACT 2600, Australia

Abstract — Advanced silicon solar cells implement complex structures on both front and rear side. Laser processing has been shown to be a versatile and cost-effective technology for such applications. Local silicon doping or contact opening via ablation are two established process steps. In this work, we investigate their influence on the quality of local contacts with a focus on contact resistivity. We determine values for ρ_c down to $70 \mu\Omega \text{ cm}^2$ and $30 \mu\Omega \text{ cm}^2$ for phosphorus and boron respectively, on a simple test structure with the help of three-dimensional numerical simulations.

Index Terms — Contact opening, contact resistivity, laser ablation, laser doping, metallization, silicon.

I. INTRODUCTION

Silicon solar cell devices have had remarkable success in the past, continuously reducing the levelized cost of electricity and already surpassing conventional power generation in some places [1, 2]. Part of this is due to the continued development of screen printed solar cells with an aluminium back-surface field (“Al-BSF”) and the ever-growing understanding of performance and loss mechanisms. Over time, various characterization techniques have proven to be a reliable source of critical information to assess the limitations of a solar cell, such as I-V characteristics, luminescence imaging or contact resistivity determination. In many places, these are accompanied by numerical device simulation, tailored for solar device simulation [3, 4].

To continue the evolution of photovoltaic devices, advanced fabrication technology and new cell architectures are employed, asking in turn for advanced characterization methods and enhanced understanding of these novel structures. One dominant loss mechanism in Al-BSF solar cells is the recombination at the rear side metal-semiconductor interface. To reduce this, passivated emitter and rear cells (PERC) have been developed [5] and are currently implemented in large scale fabrication [6]. In them, the semiconductor surface is passivated by a dielectric material and the metal-semiconductor interface is confined to a small area, reducing the area weighted recombination contribution. On the other hand, confining the contact area to a local region, enhances the impact of the contact resistivity on the total device resistive losses.

Various other advanced solar cell concepts also use dielectric layers for surface passivation. Electrodes are either created by fire-through metallization, laser fired contacts or a

local contact opening (LCO) process, e.g. mask-and-etch or laser ablation.

Another option to reduce loss mechanisms, is to create locally doped structures rather than full area doped surfaces, as long as the wafer base carrier lifetime is sufficient. For these, some options are available: full-area doping followed by mask-and-etch, masked ion implantation, local doping by a structured dopant source, e.g. printed pastes or inks, or laser doping (LD), confined to the laser spot [7].

In this work, we combine laser doping with laser ablation to create localized contacts on silicon. We test *n*- and *p*-doped areas, vary the laser doping fluence ϕ and the laser doping spot size s . We then passivate the wafer surface and create an LCO, which is slightly smaller than the LD area. Afterwards we deposit aluminium on top and anneal the system to form a local contact. We then analyse I-V measurements between local contacts and compare them to numerical device simulations, to determine the contact resistivity ρ_c , as a function of the varied parameters. Due to the ohmic behaviour of our test structure, it is easier to fabricate and analyse than previous approaches including *p-n* junctions. In the following, we refer to this method as our “ohmic local contact analysis” (OLCA).

II. EXPERIMENTAL

We utilize boron and phosphorus doped silica glass layers (BSG, PSG) as dopant sources for local laser doping (LD).

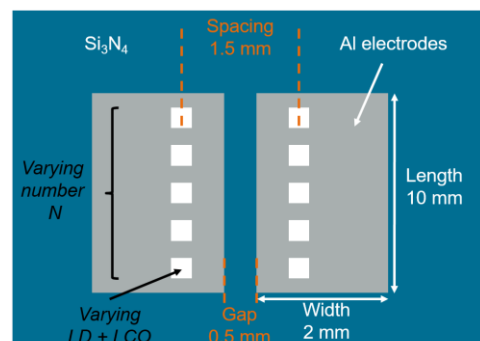


Fig. 1. Sketch of the test structure used for determination of contact resistivity. Different numbers and sizes of fabricated local contacts (white) are measured and the results are compared to numerical simulations.

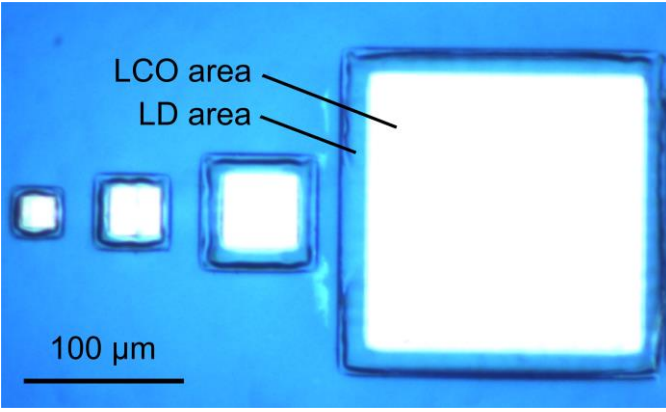


Fig. 2. Microscope image of local contacts created by laser-doping (LD) and laser-contact opening (LCO) for four different sizes, as investigated in this work.

Doped silica layers can be grown during thermal processes by oxidation of silicon wafers in an atmosphere of either $\text{BBr}_3:\text{N}_2:\text{O}_2$ or $\text{POCl}_3:\text{N}_2:\text{O}_2$. In our experiments, we perform a thermal batch process at 800°C and 750°C , respectively. LD is performed directly after the deposition with an Excimer laser source ($\lambda = 248\text{ nm}$, $\tau = 25\text{ ns}$), with variable aperture size and different laser fluences ϕ .

Subsequently, wafers are annealed in a batch process under oxygen atmosphere at 700°C for 15 min. Surfaces are capped with an 88 nm Si_3N_4 layer, deposited via low pressure chemical vapor deposition (LPCVD) at 745°C .

Local laser contact opening (LCO) is done with the same Excimer laser setup as for LD, aligned with markers on the wafer from the initial LD process. Then aluminium is evaporated and deposited on the wafer through a shadow mask to give the desired test patterns, described in the next section.

The BSG/PSG layer depositions and LD processes as well as the passivating dielectric stack were checked for homogeneity across the wafer, by photoluminescence imaging

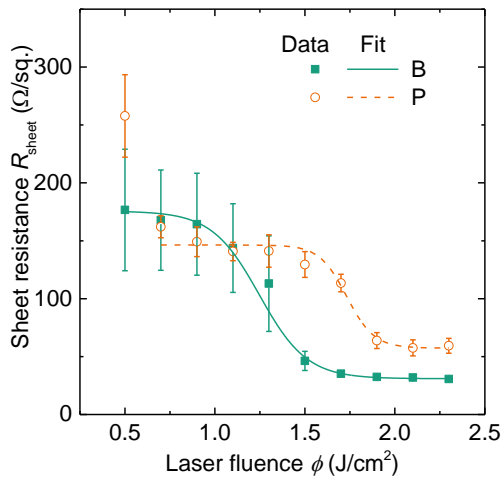


Fig. 3. Resulting sheet resistance as measured by 4pp as a function of laser fluence. The data is fitted with a sigmoidal function from Eq. (1).

(PLI). However, we did not optimize the processes for other parameters such as $j_{0,\text{pass}}$ or iV_{OC} , in this experiment. The LCO process was tested to provide minimal laser induced damage, while assuring fully opened contacts on a size of $(20\text{ }\mu\text{m} \times 20\text{ }\mu\text{m})$. We evaluate the local laser-doped contact properties on two different sample sets, described in the following.

A. Laser doping parameters

In our first experiments, we characterize the laser doping parameters by stitching large spots ($500\text{ }\mu\text{m} \times 500\text{ }\mu\text{m}$) on $1000\text{ }\Omega\text{ cm}$, $4''$, n-type Fz-Si, wafers with a thickness of $400\text{ }\mu\text{m}$. We measure sheet resistance R_{sheet} by four point probe (4pp) and doping profiles $n(z)$ via electrochemical C-V measurements (ECV). We use these values, as the independent LD parameters in our subsequent analysis, where we confine the LD to much smaller sizes.

We also measure the PL signal of laser doped regions and determine the recombination parameter j_0 by calibrating the signal to a reference quasi-steady state photoconductance (QSSPC) measurement on the same wafer [8], to extract the dominating recombination contribution after LD. The results of this study are published elsewhere [9].

B. Contact resistivity of local contacts

For the determination of contact resistivity, we use $1.4\text{ }\Omega\text{ cm}$, Cz-Si wafers with a thickness of $300\text{ }\mu\text{m}$. We select the same polarity for wafer base doping and local contacts, so that the structure is purely ohmic and measure the I-V characteristic, to determine the total resistance between two rows of local contacts.

In the experiment, we align the local contacts collinear and equidistant in a row under an Al-electrode. We then place a similar contact row and electrode in a distance of 1.5 mm between the center of the two contact rows, as sketched in Fig. 1. We vary the laser fluence ϕ , number of contacts under the electrodes N , spot size s and confine the LCO size c to a region smaller than the LD regions (s. Fig. 2).

Then we simulate each of the geometrically different structures (N, s, c) with Quokka 3 [4], while sweeping different values of ρ_c for each configuration. We afterwards plot simulation and measurement and compare the results to determine the contact resistivity ρ_c . Where necessary, we repeat the simulation, to better match the measured values with new ρ_c .

III. RESULTS

We measure the resulting sheet resistance after large-area laser doping for a variety of different laser fluences from a single pulse process. The averaged measurements are displayed in Fig. 3.

For both doping species, we find a strong decrease after a certain threshold fluence ϕ_0 . We thus fit R_{sheet} around the

TABLE I
RESULTS OF LOCAL LASER DOPED CONTACTS

ϕ J/cm ²	Boron	Phosphorus
	R_{sheet} Ω/\square	R_{sheet} Ω/\square
0.9	277 ± 56	
1.3	97 ± 9	186 ± 20
1.5	47 ± 2	164 ± 14
1.7	36 ± 4	130 ± 41
2.1	36 ± 4	60 ± 7

steepest drop in the sheet resistance with a sigmoidal function ('dose-response') of the form

$$R_{\text{sheet}}(\phi) \cong R_{\text{min}} + \frac{(R_{\text{max}} - R_{\text{min}})}{1 + 10^{(\phi_0 - \phi)p}}. \quad (1)$$

Here R_{min} and R_{max} are the minimum and maximum measured sheet resistance, and p is a parameter describing the steepness of the drop. We extract the position of the threshold fluence from the fit to be $\phi_{0,p} \approx 1.7 \text{ J/cm}^2$ and $\phi_{0,B} \approx 1.3 \text{ J/cm}^2$. The goodness of fit $R^2 > 0.96$ indicate a reasonable description of our data.

For the fabrication of local contacts, we choose four different fluences for laser doping of boron and phosphorus each. The doping profiles are shown in Fig. 4. For phosphorus doping (open symbols), the three lower fluences ($< \phi_{0,p}$) have a similar surface concentration n_{Surf} and vary only slightly but ascending in depth z_0 . For 2.1 J/cm^2 ($> \phi_{0,p}$), both n_{Surf} and z_0 are significantly increased. The same is true for the boron profiles with respect to $\phi_{0,B}$. The sheet resistances for both dopants and all fluences are listed in Tab. 1.

In standard solar cells, the contact resistivity is commonly determined by the "Transfer-Length-Method" (TLM) [11]. For this, I - V measurements between similar collinear electrodes on top of an emitter diffusion are performed for

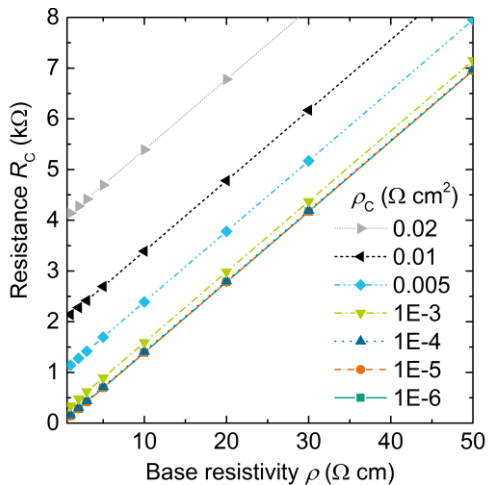


Fig. 5. Quokka 3 simulation of base resistivity significance for our test structures.

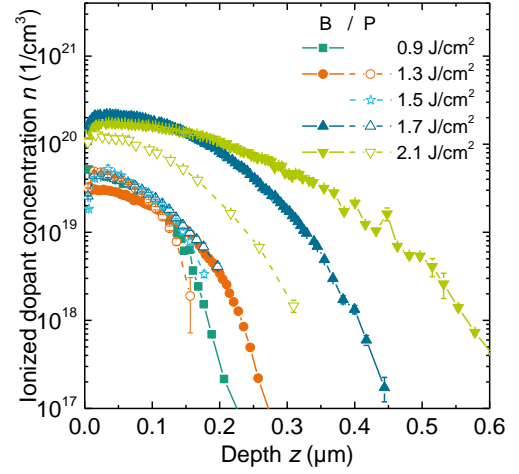


Fig. 4 Dopant profiles for different laser fluences. Open symbols phosphorus, solid symbols boron. Higher fluences result in higher surface concentration and depth. Strong increase around a specific fluence as shown in Fig. 3, depending on dopant species.

varying distance d . Then, the determined total resistance can be plotted as a function of distance d , and the contact resistance R_C is the result of a linear fit, evaluated at $d = 0$. The contact resistivity ρ_C is then calculated by normalizing R_C to the contact area.

For this approach to be valid, several assumptions have to be made: electrodes have to be similar in terms of contact area and contact resistivity to normalize the results. Also, the presence of a uniform emitter sheet resistance between the electrodes is important, as it confines the current flow to a small layer. If no other contribution has a dominant influence on the I - V measurement, the slope is only defined by the emitter sheet resistance and width of the test structure.

The advantage of this method is that it can be easily applied in standard solar cells, as the equidistant front metal grid can be used for the desired test structure.

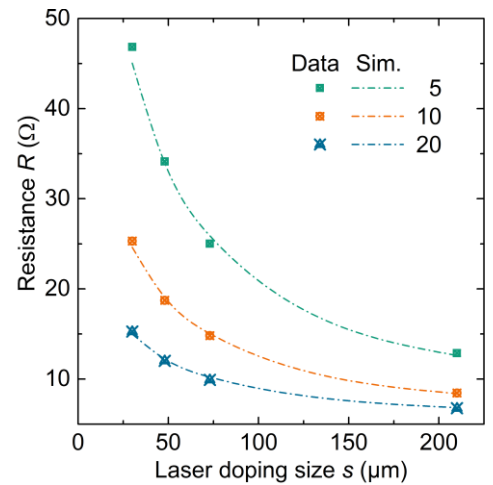


Fig. 6. Consistency check, where only data for small spots has been used to determine ρ_C yet the other measurements meet the simulation results.

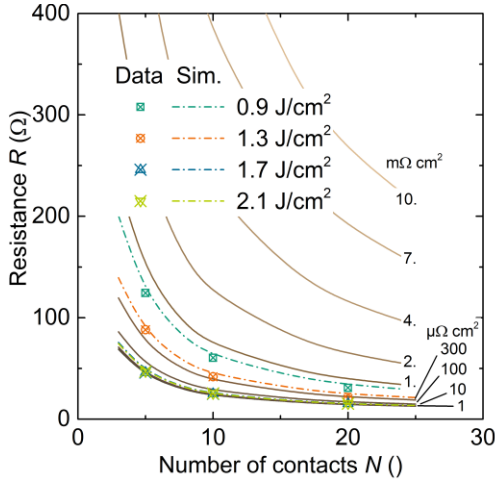


Fig. 7. Data for B doped samples after FGA at 300 °C, $s = 30 \mu\text{m}$. Straight lines for ρ_c as labelled, dashed lines ρ_c as in Tab. 1. Higher laser fluences results in lower ρ_c . The lowest measured values are approaching the sensitivity of the method predicted by the simulation.

For the localized contacts in our structure, this simple analysis approach cannot be used, as no uniform emitter doping is present to confine the current flow to a thin layer. In our OLCA, the actual current flow and the measured resistance strongly depends on localized effects such as current crowding. Therefore, we perform full-size three-dimensional simulations of our structures and determine the contact resistivity of the local contacts ρ_c by fitting the measured total resistance values.

In similar attempts, others have chosen to measure local contacts by the p - n junction characteristic, where the base contact has to have a very low contact resistivity and is therefore also highly doped [8, 10]. To minimize the fabrication effort, we decided to fabricate the n -type contacts on n -type wafer material and p -type contacts on p -type wafers. In this setup the structure is purely ohmic and can be simulated by Quokka 3 [13]. To determine the sensitivity of parameters other than ρ_c , we performed some initial sweeps in the simulation.

We find that the wafer base resistivity has a significant impact on the total resistance measurement, as it linearly correlates with this quantity (Fig. 5). We also observe that there is a lower limit for the values of ρ_c , which can be distinguished by this method. In order to minimize the error in base resistivity, we measure the wafer base doping by an inductive coil at several locations over the wafer prior metallization for each wafer.

We perform a sensitivity analysis for sheet resistance and local contact size of the local contacts. As expected, the sheet resistance does not affect the total resistance, due to the small area fraction of the laser-doped regions. However, the contact size has a significant influence on the total resistance. Smaller contact sizes lead to a higher total resistance and increase the

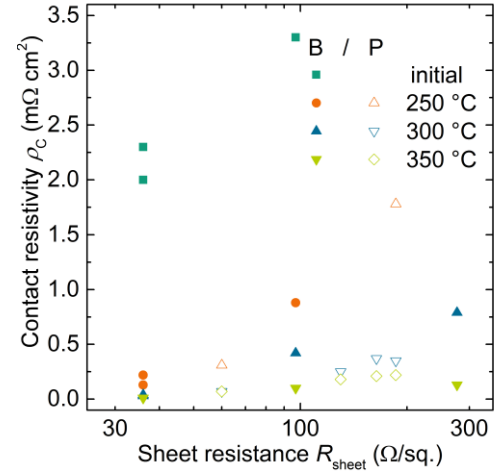


Fig. 8. Contact resistivity for B and P doped localized contacts, as a function of the sheet resistance. Only values for linear contacts are listed. Values are in agreement with comparable literature values for large area diffusions.

sensitivity to the contact resistivity (s. Fig. 6, lines). Note that the simulations assume perfect and homogeneous contacts and total resistance measurement can in principle be affected by local non-uniformities. In Fig. 6, we also plot the measured resistance R against s , for a doping fluence of $\phi = 2.1 \text{ J/cm}^2$ after the same 300 °C FGA. Here, ρ_c was derived from the first data points at a size of $s = 30 \mu\text{m}$, *i.e.* the matching curve in Fig. 7, and only s was varied in the simulation. Yet the data and simulation coincide very well, underlining the feasibility of the method and the homogeneous character of our contacts.

When measuring the contact resistivity, we ensure the insulating properties of the dielectric stack by measuring a pair of reference electrodes without local contacts for each set of parameters, to ensure that the structure is only contacted through the laser-doped contacts.

We determine ρ_c for both dopant types by comparing experiment (Fig. 7, marker) and simulation (Fig. 7, lines) and then perform additional simulations (Fig. 7, dashed lines) to find a closer match. The exemplary set of measurements shown, has been taken for different boron doped contacts after a forming gas anneal (FGA) at 300 °C. We excluded measurements with non-ohmic I-V characteristics from our analysis which we observed for some laser doping parameters below a certain annealing temperature. We observed that boron contacts tend to require lower annealing temperatures to form ohmic contacts to the used PVD aluminium (not shown). We plot all extracted contact resistivities in Fig. 8 as a function of the determined sheet resistance for the used laser doping parameters, after different annealing steps. The first two annealing steps (250 °C and 300 °C) have a strong influence, reducing the determined contact resistivity. Afterwards the difference is smaller. There is a small dependency with the sheet resistance, which gets smaller for higher annealing steps.

V. SUMMARY AND OUTLOOK

For both dopants, very low contact resistivities could be obtained by PVD aluminium and annealing at 300 °C and above.

A clear distinction for induced sheet resistance and accompanying contact resistivity has been found, around a threshold fluence ϕ_0 . The obtained values for ρ_C are in good agreement with literature values from Schroder [11] or Fong [12], where evaluations have been performed using full area dopings and the TLM method. Besides the smaller contact area, the usage of localized contacts therefore did not show an adverse effect in our experiment.

The usage of laser doping, potentially allows for further inside into the critical parameters of contact formation, by tailoring different dopant profiles. Alternatively, microanalysis of the contacts could be performed.

In accompanying studies it has been shown that increased laser doping fluences, which showed lowest contact resistivities here, lead to higher recombination due to laser damage. As both quantities need to be optimized by experiments, the presented structure allows for an easier sample fabrication. The approach should be transferable to other types of localized contacts (i.e. without LD), as long as the real size can be precisely determined.

ACKNOWLEDGEMENTS

This Program has been supported by the Australian Government through the Australian Renewable Energy Agency (ARENA). Responsibility for the views, information or advice expressed herein is not accepted by the Australian Government.

The authors would like to thank colleagues at ANU for assistance in sample preparation and process realization, the technical staff for their support of the PV labs and all coworkers involved in discussions.

J.D.H acknowledges funding by the center of renewable energy of the University of Freiburg, within the interdisciplinary graduate school “DENE”.

REFERENCES

- [1] International Renewable Energy Agency (IRENA), “Renewable Power Generation Costs in 2017,” 2018.
- [2] Fraunhofer Institute for Solar Energy Systems (ISE), “Studie: Stromgestehungskosten erneuerbare Energien (März 2018),”
- [3] Pietro P. Altermatt, Yang Yang, Daming Chen, Yifeng Chen, Zhiqiang Feng, Pierre Verlinden, “A method for optimizing PERC cells in industrial production lines by using final IV parameters, statistical procedures and numerical device modeling,” in *SiliconPV 2018*.
- [4] S. Wasmer and J. Greulich, “Modelling and analysis of solar cell efficiency distributions,” (en), *Jpn. J. Appl. Phys.*, vol. 56, no. 8S2, 08MB02, <http://iopscience.iop.org/article/10.7567/JJAP.56.08MB02/pdf>, 2017.
- [5] A. W. Blakers, A. Wang, A. M. Milne, J. Zhao, and M. A. Green, “22.8% efficient silicon solar cell,” *Appl. Phys. Lett.*, vol. 55, no. 13, p. 1363, 1989.
- [6] VDMA, “International Technology Roadmap for Photovoltaic (ITRPV),” Ninth Edition 2018, 2018. [Online] Available: <http://www.itrpv.net/>.
- [7] M. Ernst *et al.*, “Fabrication of a 22.8% Efficient Back Contact Solar Cell With Localized Laser-Doping,” *Phys. Status Solidi A*, vol. 214, no. 11, p. 1700318, 2017.
- [8] M. Ernst, A. Fell, E. Franklin, and K. J. Weber, “Characterization of Recombination Properties and Contact Resistivity of Laser-Processed Localized Contacts From Doped Silicon Nanoparticle Ink and Spin-On Dopants,” *IEEE J. Photovoltaics*, vol. 7, no. 2, pp. 471–478, 2017.
- [9] M. Ernst, J. D. Huyeng, K. C. Fong, D. Walter, and A. W. Blakers, “Unravelling the origins of contact recombination for localized laser-doped contacts,” in *WCPEC 7 (2018)*.
- [10] A. Fell, S. Surve, E. Franklin, and K. J. Weber, “Characterization of Laser-Doped Localized p-n Junctions for High Efficiency Silicon Solar Cells,” *IEEE Trans. Electron Devices*, vol. 61, no. 6, pp. 1943–1949, 2014.
- [11] D. K. Schroder and D. L. Meier, “Solar cell contact resistance—A review,” *IEEE Trans. Electron Devices*, vol. 31, no. 5, pp. 637–647, 1984.
- [12] K. C. Fong *et al.*, “Contact Resistivity of Evaporated Al Contacts for Silicon Solar Cells,” *IEEE J. Photovoltaics*, vol. 5, no. 5, pp. 1304–1309, 2015.
- [13] A. Fell, J. Schön, M. C. Schubert, and S. W. Glunz, “The concept of skins for silicon solar cell modeling,” *Sol. Energy Mater. Sol. Cells*, vol. 173, pp. 128–133, 2017.